https://doi.org/10.5194/acp-2019-1063
Preprint. Discussion started: 3 December 2019

Atmospheric Chemistry and Physics Discussions
Open Access
EGU

Effects of Liquid Phase Cloud Microphysical Processes in Mixed Phase Cumulus Clouds over the Tibetan Plateau

Xiaoqi Xu[1], Chunsong Lu[1*], Yangang Liu[2], Wenhua Gao[3], Yuan Wang[1], Yueming Cheng[1], Shi Luo[1], Kwinten Van Weverberg[4]

1. Key Laboratory for Aerosol-Cloud-Precipitation of China Meteorological Administration/Collaborative Innovation Center on Forecast and Evaluation of Meteorological Disasters (CIC-FEMD), Nanjing University of Information Science & Technology, Nanjing, China
2. Environmental and Climate Sciences Department, Brookhaven National Laboratory, Upton, US
3. State Key Laboratory of Severe Weather, Chinese Academy of Meteorological Sciences, Beijing, China
4. Met Office, Exeter, UK

* Correspondence: luchunsong110@gmail.com

https://doi.org/10.5194/acp-2019-1063
Preprint. Discussion started: 3 December 2019

Atmospheric Chemistry and Physics Discussions

Abstract

Overprediction of precipitation over the Tibetan Plateau is often found in numerical simulations, which is thought to be related to coarse grid sizes or inaccurate large-scale forcing. In addition to confirming the important role of model grid sizes, this study shows that liquid-phase precipitation parameterization is another key culprit, and underlying physical mechanisms are revealed.

A typical summer plateau precipitation event is simulated with the Weather Research and Forecasting (WRF) model by introducing different parameterizations of liquid-phase microphysical processes into the commonly used Morrison scheme, including autoconversion, accretion, and entrainment-mixing mechanisms. All simulations can reproduce the general spatial distribution and temporal variation of precipitation. The precipitation in the high-resolution domain is less overpredicted than in the low-resolution domain. The accretion process plays more important roles than other liquid-phase processes in simulating precipitation. Employing the accretion parameterization considering raindrop size makes the total surface precipitation closest to the observation which is supported by the Heidke skill scores. The physical reason is that this accretion parameterization can suppress fake accretion and liquid-phase precipitation when cloud droplets are too small to initiate precipitation.

https://doi.org/10.5194/acp-2019-1063
Preprint. Discussion started: 3 December 2019

1. Introduction

The Tibetan Plateau (TP) is the highest and largest plateau of the world with an average elevation of more than 4 km above the sea level and an area larger than 2.5×10^6 km^2. Its active exchanges of heat and moisture have significant influences on climate and environmental change, not only in China but also over East Asia and even the entire northern hemisphere through strong thermal and dynamic forcing (Yeh, 1950; Flohn, 1957; Hahn and Manabe, 1975; Ye, 1981; Wu and Chen, 1985; Yanai et al., 1992; Ding et al., 2001; Wang et al., 2008; Molnar et al., 2010; Yang et al., 2014). Many studies have reported that the tropospheric heating over the TP has decisive effects on the maintenance of the Asian summer monsoon (Luo and Yanai, 1983, 1984; Ueda and Yasunari, 1998). The upward transport of sensible heat and the release of latent heat over the plateau region due to convective clouds are important heat sources in the upper troposphere, driving the East Asian summer monsoon and associated precipitation (Nitta, 1983; Luo and Yanai, 1984; Yanai and Li, 1994; Ueda et al., 2003; Hsu and Liu, 2003).

During the summer monsoon, deep convection develops over the TP with a marked diurnal cycle in precipitation (Fujinami and Yasunari, 2001; Kurosaki and Kimura, 2002; Chen et al., 2017a), frequently associated with mesoscale vortices (Shen et al., 1986; Wang et al., 1993; Li et al., 2008). Overall, summer precipitation on the plateau is characterized by frequent, but rather weak convection (Gao et al., 2016). Undoubtedly, these characteristics are heavily influenced by the unique terrain of the

https://doi.org/10.5194/acp-2019-1063
Preprint. Discussion started: 3 December 2019

TP (Porcù et al., 2014; Chen et al., 2017b;Wu and Liu, 2017).

The particularity of the TP has led it to be one of the most challenging areas for precipitation simulation. Precipitation simulated with coarse resolution (>3km) is often found to be higher than observations (Maussion et al., 2011; Xu et al., 2012; Gao et al., 2016). Some studies claimed that low resolution was responsible for the overprediction of precipitation (Sato et al., 2008; Xu et al., 2012). Sato et al. (2008) also showed that a finer resolution simulation was more efficient in reproducing the diurnal variation of summer precipitation. Maussion et al. (2011) investigated effects of different physical schemes and found a strong microphysical sensitivity for convective precipitation, but much smaller sensitivity for simulations with dominant advection over the TP. Gerken et al. (2013) compared simulations with different forcing data and found that there were large differences in the precipitation generated from different initial and boundary conditions. Some studies also claimed that elevated aerosol concentrations can remarkably enhance convections due to specific topography of the TP, however, few studies focus on this issue (Zhou et al., 2017) which was broadly investigated in other areas (e.g. Wang et al., 2011; Fan et al., 2018).

The high elevation of the TP, and hence the typically low melting level, enables plenty of supercooled liquid water, even in summer (Gao et al., 2016; Zhao et al., 2017; Tang et al., 2019). Hence, it is likely that liquid precipitation processes play a role in the precipitation overestimation in this region. For instance, Zhao et al. (2017) confirmed that supercooled cloud water dominated in precipitating cumulus clouds over

https://doi.org/10.5194/acp-2019-1063
Preprint. Discussion started: 3 December 2019

the Naqu area at the temperature of -2.5 to -3.5°C. By analyzing the raindrop size distribution at Maqu over the TP , Li et al. (2006) argued that the liquid-phase processes were important for surface precipitation, although ice-phase rain processes dominated over the region. Gao et al. (2016) investigated the roles of liquid-phase rain microphysical processes and suggested that liquid-phase rain processes could be important over the precipitation centers during weak convection over the TP.

Three parameterized liquid-phase processes are investigated in this paper: autoconversion, accretion, and entrainment-mixing. Autoconversion is expressed as the mass conversion rate from cloud to rain due to the collision-coalescence of cloud droplets while accretion is defined as the rate of mass conversion from cloud to rain due to the collection of cloud droplets by raindrops. The sum of autoconversion and accretion is calculated as the total mass conversion from cloud to raindrop populations during the collision-coalescence process (Wood, 2005a). Wang et al. (2012) and Gettelman et al. (2013) highlighted that autoconversion was important for the initiation of precipitation whereas accretion was responsible for the amount of precipitation. The process of entrainment and mixing between cloud and environment is one of the most uncertain processes in cloud physics. The key issue of the entrainment-mixing process is whether evaporation due to mixing causes a reduction of only droplet size (homogeneous mixing), only droplet number (extremely inhomogeneous mixing), or both. Therefore, different entrainment-mixing mechanisms can affect cloud microphysical properties and hence cloud-related processes such as radiation and precipitation (Lasher-Trapp et al., 2005; Grabowski, 2006; Chosson et al., 2007; Slawinska et al., 2008; Lu et al., 2013;Cooper et al., 2013).

So far, it is still unknown how the above three liquid-phase processes affect precipitation over the TP and whether improving the parameterizations of these three liquid-phase processes can mitigate the problem of overpredicted precipitation. Further unknown is the relative contributions of these three processes to surface precipitation over the TP and which of these parameterized processes exhibits the largest sensitivity in terms of surface precipitation. This study fills these gaps by comparing simulations of a precipitation event over the TP with different liquid-phase parameterizations and dissecting the underlying physical mechanisms.

This paper is organized as follows: A brief introduction on the precipitation event and experimental setup are given in section 2. Section 3 discusses the influence of liquid-phase processes on cloud microphysics, radiation, and precipitation in different numerical experiments. Summary and conclusions are given in section 4.

2. Description of precipitation event and observational dataset

2.1 Case description and observations

As mentioned in Gao et al. (2016), the entire plateau experienced a large frontal system from 21 to 23 July 2014 and observed precipitation initiated at 0400 UTC (Coordinated Universal Time) 22 July. The simulations are compared against the data derived from multiple satellite precipitation data sets and blended using a dynamic

https://doi.org/10.5194/acp-2019-1063
Preprint. Discussion started: 3 December 2019

Bayesian model averaging (BMA) algorithm in regions with sparse gauge observations, proposed by Ma et al. (2018). This new precipitation dataset is more viable for complex terrains such as the TP region. Hence, observations should be more accurate and have higher spatial (0.1°) and temporal (1h) resolution than the Tropical Precipitation Measuring Mission (TRMM) usually used in this region (Fu et al., 2007; Yin et al., 2008; Maussion et al., 2011; Xu et al., 2012).

2.2 Model and experiment description

The Weather Research and Forecasting (WRF) model version 3.8.1 is used to simulate this typical summer TP precipitation event. The WRF model is a next-generation mesoscale numerical weather prediction system designed for both atmospheric research and operational forecasting applications. Here, WRF is used as a cloud-resolving model with 1 km horizontal grid spacing for the innermost domain (referred to as domain 03) with 276×276×45 grid points, which covers most of the plateau center; the spatial resolutions for the two outer domains (01 and 02) are 25 km and 5 km with 200×200×45 and 176×176×45 grid points, respectively (Figure 1). Initial and boundary conditions are provided by the National Centers for Environmental Prediction Final operational global analysis data with 1° spatial and 6 h temporal resolution. The simulation starts at 1200 UTC 21 July and ends at 0000 UTC 24 July, with a total of 60 h integration time. We focus on the results of the last 48 h from domain 02 and domain 03 with a 30-minute interval.

https://doi.org/10.5194/acp-2019-1063
Preprint. Discussion started: 3 December 2019

Atmospheric Chemistry and Physics Discussions

The microphysics scheme used in the control run is the Morrison double-moment scheme Morrison and Grabowski, 2008. Note that this bulk scheme is different from the default version released in the WRF model with a fixed cloud droplet number concentration (N_c) (e.g. N_c = 250 cm^{-3}). This version can predict the number concentration and mass mixing ratios of cloud droplets (N_c, q_c), raindrops (N_r, q_r), ice crystals (N_i, q_i), snow particles (N_s, q_s), and graupel particles (N_g, q_g). The main liquid-phase conversion processes, i.e. autoconversion (R_{auto}; kg m^{-3}s^{-1}) and accretion (R_{accr}; kg m^{-3}s^{-1}), are both based on Khairoutdinov and Kogan (2000), further referred to as the KK schemes:

$$R_{\mathrm{auto}} = 1350 \times q_{\mathrm{c}}^{2.47}(N_{\mathrm{c}} \times 10^{-6})^{-1.79}\rho_{\mathrm{a}}^{-1.47}, \quad (1)$$

$$R_{\mathrm{accr}} = 67 \times (q_{\mathrm{c}}q_{\mathrm{r}})^{1.15}\rho_{\mathrm{a}}^{-2.3}, \quad (2)$$

where ρ_{a} is the air density.

To explore the influences of liquid-phase cloud microphysical processes in mixed-phase clouds, we implement several different expressions for autoconversion, accretion, and entrainment-mixing process into the Morrison scheme, and examine the model sensitivity. In addition to the default KK schemes, three commonly-used autoconversion schemes are employed and referred to as Be68, Bh94, and LD04 for convenience, respectively:

1) Berry (1968):

$$R_{\mathrm{auto}} = \frac{3.5\times10^{-2}q_{\mathrm{c}}^{2}}{0.12+1.0\times10^{-12}\frac{N_{\mathrm{c}}}{q_{\mathrm{c}}}}, \quad (3)$$

This is the default scheme in several global climate models such as Model for

https://doi.org/10.5194/acp-2019-1063
Preprint. Discussion started: 3 December 2019

Interdisciplinary Research on Climate version 5 (MIROC5; Michibata and Takemura, 2015; Jing and Suzuki, 2018)

2) Beheng (1994):

$$R_{\mathrm{auto}} = 6.0 \times 10^{28} n^{-1.7} (q_{\mathrm{c}} \times 10^{-3})^{4.7} (N_{\mathrm{c}} \times 10^{-6})^{-3.3}, \quad (4)$$

where n is set to 10 in Eq.4, which is related to the width of cloud droplet size distribution;

3) Liu and Daum (2004):

$$R_{\mathrm{auto}} = P_0 T , \quad (5a)$$

$$P_0 = 1.1 \times 10^{13} \left[\frac{(1+3\varepsilon^2)(1+4\varepsilon^2)(1+5\varepsilon^2)}{(1+\varepsilon^2)(1+2\varepsilon^2)} \frac{q_{\mathrm{c}}^3}{N_{\mathrm{c}}} \right], \quad (5b)$$

$$T = \frac{1}{2}(x_{\mathrm{c}}^2 + 2x_{\mathrm{c}} + 2)(1 + x_{\mathrm{c}}) e^{-2x_{\mathrm{c}}}, \quad (5c)$$

$$x_{\mathrm{c}} = 9.7 \times 10^{-14} N_{\mathrm{c}}^{3/2} q_{\mathrm{c}}^{-2}. \quad (5d)$$

The LD04 derived by Liu and Daum (2004) and Liu (2005) considers relative dispersion ε (the ratio of the standard deviation to the mean radius) in addition to droplet concentration and liquid water mixing ratio. This scheme was implemented into the WRF double-moment schemes (Xie and Liu, 2011; Xie et al., 2013). P_0 and T represent rate function and threshold function, respectively; the ε is set to 0.4 as the average value based on Zhao et al. (2006) and Wang et al. (2019).

Considering that most accretion schemes only take mass mixing ratios of cloud droplets and raindrops (i.e. q_{c} and q_{r}) into account, a parameterization that relates the accretion process to liquid droplets number concentration and drop size distribution is adopted from Cohard and Pinty (2000), named as CP2k:

https://doi.org/10.5194/acp-2019-1063
Preprint. Discussion started: 3 December 2019

Atmospheric Chemistry and Physics Discussions

$$R_{\mathrm{accr}} = \frac{\pi}{6}\rho_{\mathrm{W}}\rho_{\mathrm{a}}K_1\frac{N_{\mathrm{c}}N_{\mathrm{r}}}{\lambda_{\mathrm{c}}^3}\left(\frac{A_1}{\lambda_{\mathrm{c}}^3}+\frac{B_1}{\lambda_{\mathrm{r}}^3}\right),$$

$$if\ R_{\mathrm{r}} \geq 50\ \mu m, \text{and} \tag{6a}$$

$$R_{\mathrm{accr}} = \frac{\pi}{6}\rho_{\mathrm{W}}\rho_{\mathrm{a}}K_2\frac{N_{\mathrm{c}}N_{\mathrm{r}}}{\lambda_{\mathrm{c}}^3}\left(\frac{A_2}{\lambda_{\mathrm{c}}^6}+\frac{B_2}{\lambda_{\mathrm{r}}^6}\right),$$

$$if\ R_{\mathrm{r}} < 50\ \mu m, \tag{6b}$$

where ρ_{W} is the water density, R_{r} is the raindrop radius, K_1 and K_2 are empirical constants; the subscripts *c* and *r* denote cloud droplets and raindrops, respectively. A_1, A_2, B_1, and B_2 are the functions related to two dispersion parameters of the gamma size distribution; λ is the slope parameter and is derived from the dispersion parameter, number concentration and mixing ratio of the species (see Morrison et al., 2005). Due to specified dispersion parameters for raindrops, $\lambda_{\mathrm{r}} = (\pi\rho_{\mathrm{W}}N_{\mathrm{r}}/q_{\mathrm{r}})^{1/3}$ which is inversely proportional to the radius of the raindrops. Another accretion scheme (Ko13, Kogan, 2013) is also tested:

$$R_{\mathrm{accr}} = 8.53 \times q_c^{1.05} q_r^{0.98} \rho_a^{-2.03}, \tag{7}$$

For the entrainment-mixing process, the subgrid-scale mixing can be defined using a single parameter α in this microphysical scheme (Morrison and Grabowski, 2008; Lu et al., 2013):

$$N_c = N_{\mathrm{c0}}\left(\frac{q_{\mathrm{c}}}{q_{\mathrm{c0}}}\right)^{\alpha}, \tag{8}$$

where the N_{c} and N_{c0} are the number concentrations of cloud water droplets after and before the evaporation process, respectively, and the q_{c} and q_{c0} represent the corresponding mixing ratios, respectively. The parameter α can set to be any value between 0 and 1 corresponding to a different degree of the subgrid-scale mixing

https://doi.org/10.5194/acp-2019-1063
Preprint. Discussion started: 3 December 2019

Atmospheric Chemistry and Physics Discussions

homogeneity. When α = 0, homogeneous mixing is assumed (the control run). On the contrary, when α = 1, extremely inhomogeneous mixing is assumed (the INHOMO run).

In total, we have 7 simulations: the control run with the KK schemes for autoconversion and accretion, and homogeneous mixing mechanism, and sensitivity tests with three autoconversion schemes (Be68, Bh94 and LD04), two accretion schemes (CP2k and Ko13), and one entrainment-mixing scheme (INHOMO).

3. Results

3.1 Control run

3.1.1 Precipitation from the control run and observations

Result of 48 h accumulated precipitation over domain 02 (Figure2b) rather than domain 03 (Figure 2d) is used to compare with observations (Figures 2a and c) because the domain resolution of 5 km is closer to that of the observation data (0.1°). The precipitation from 0000 UTC 22 July to 0000 UTC 24 July 2014 from the control run is averaged to fit the resolution of 0.1°. The results indicate that the control run can reproduce the primary rainband oriented in the northeast-southwest direction. The precipitation in most regions is less than 50 mm and the maximum value is approximately 80 mm in the observation. Although the control run is spatially consistent with the observation, the maximum precipitation in simulation is about 200 mm, over twice of the observation. Similar biases were reported in Xu et al. (2012) and Gao et al. (2016); these inconsistencies could be related to the large-scale dynamic

https://doi.org/10.5194/acp-2019-1063
Preprint. Discussion started: 3 December 2019

Atmospheric Chemistry and Physics Discussions
Open Access
EGU

forcing or the model resolution. For domain 03, when the simulated precipitation is averaged to 0.1°, there are only about 27*27 data points; the data quantity may not be big enough to compare the spatial distribution of precipitation between simulations and observations. This could explain the spatial precipitation bias shown in Figures 2c and 2d. Besides spatial comparison, Figures 3a and 3b show the temporal evolutions of area-averaged hourly precipitation rate from the observation and the control run over domain 02 and domain 03, respectively. The black solid lines denote the observation data. The simulations of both domains correlate well with observations in trends, but the domain 03 is clearly closer to the observations in terms of precipitation rate. Similar to previous studies (e.g. Xu et al., 2012), the precipitation of domain 02 with a low resolution is overestimated compared to the observations. The observations for domain 03 show that there are two peaks of precipitation in the local afternoon (UTC + 6 h). The first precipitation event starts from 0400 UTC 22 and ends at 1800 UTC with the maximum precipitation rate of 1.0 mm/h attained at 0900 UTC. The other precipitation peak is weak with the maximum precipitation rate of only about 0.4 mm/h. The control run shows a slightly smaller precipitation rate than the observation for the first peak and a slightly larger rate for the second peak. The time of the peaks in the simulations is about 2 hours later than that in the observations, which was also reported in Gao et al. (2018). Generally speaking, the control run captures the main features of the precipitation evolution (the peaks and the trend) but also produces an artificial weak peak (~0.2 mm/h) at about 0000 UTC 23 which is not observed.

3.1.2 Microphysical processes in the control run

Based on the precipitation mentioned above, the microphysics is examined for different resolutions/periods. For domain 02, considering that the altitude of the southeastern corner is lower than the other regions, liquid-phase precipitation is expected to be stronger. Therefore, domain 02 is divided into two parts: the southeastern corner and the other regions. For domain 03, the two precipitation peak periods are studied separately.

Figure 4 shows the mean vertical profiles of five types of hydrometeors and their primary microphysical processes for the two separate regions over domain 02 and the two precipitation peaks (5 hours) over domain 03, respectively. For domain 02, mixing ratios of ice-phase hydrometeors (ice, snow, and graupel) and rates of microphysical processes (RIM-s, RIM-g, MELT) over the southeastern corner (Figures 4c and d) are generally equivalent to or smaller than those over the other regions (Figures 4a and b). Mixing ratios of liquid-phase hydrometeors (cloud and rain) and microphysical processes (ACCR-r, AUTO-r) are larger over the southeastern corner than those over the other regions. As mentioned above, liquid droplets have more opportunities to grow over the southeastern corner because of its lower terrain. For domain 03, mixing ratios of ice-phase hydrometeors (ice, snow, and graupel) and rates of microphysical processes (EVAP-r, ACCR-s, RIM-s, RIM-g, MELT) are smaller during the second peak period (Figures 4g and h) than those during the first peak period (Figures 4e and

https://doi.org/10.5194/acp-2019-1063
Preprint. Discussion started: 3 December 2019

f). However, accretion rate of cloud droplets by rain (ACCR-r) is larger for the second peak than for the first one, although melting is still dominant. Therefore, the liquid-phase processes over the southeastern corner in domain 02 and the second precipitation peak in domain 03 are more important than those over the other regions in domain 02 and the first precipitation peak in domain 03, respectively, though the reasons are different. While ice phase processes are equally important across the entire domain 02, the warmer temperatures in the lower southeastern corner allow for more liquid phase precipitation. In domain 03, however, the second peak is clearly associated with smaller ice-related conversion rates.

3.2 Sensitivity tests with different parameterizations of liquid-phase processes

Besides the control run, precipitation, microphysical properties, and their related processes from the sensitivity simulations are discussed in this section, including Be68, Bh94, LD04, CP2k, Ko13, and INHOMO.

3.2.1 Precipitation from the sensitivity tests and observations

The results of precipitation from the sensitivity tests are shown in Figures 5 and 6. All simulation cases have produced the similar rain band/trend and precipitation rate, compared to the control run, except the CP2k experiment. The CP2k has distinctly weaker precipitation than the other simulations especially over the southeastern corner in domain 02 and during the second precipitation peak period in domain 03.

https://doi.org/10.5194/acp-2019-1063
Preprint. Discussion started: 3 December 2019

Qualitatively, the results from the CP2k are closer to the observations (Figures 2, 3, 5 and 6).

The Heidke skill score (HSS) is used to quantitatively evaluate the simulations with different schemes:

$$\mathrm{HHS} = \frac{2(ad - bc)}{(a + c)(c + d) + (a + b)(b + d)}, \quad (9)$$

where the four elements *a*-*d* for HSS, representing the numbers of "hits", "false alarms", "misses" and "correct negatives", respectively, are calculated from a contingency table (Table 1). HHS can not only judge well-simulated events (both hits and correct negatives, element *a* and *d*) but also account for erroneous forecast (*b* and *c*) (Barnston, 1992). A higher HSS (0 ~ 1) represents better skill. As shown in Table 1, p_t is the threshold value and is set to be 2 mm covering most of the observed and simulated precipitation area, p_s and p_o are the values from simulations and observations, respectively.

The elements a-d and HSS for all sensitivity tests over domain 02 and 03 are shown in Table 2. All the cases in domain 02 have the HSS scores exceeding 0.4 and are close to each other except for the CP2k. The impacts of changing autoconversion schemes and mixing mechanisms on HSS are limited. The CP2k accretion scheme, however, has significantly higher HSS than other cases, particularly due to its high value of d, the "correct negatives" mainly over the southeastern region for domain 02. The high HSS scores in the CP2k indicate that changing the accretion scheme is a possible way to improve the much-overestimated precipitation in simulations over this region. The HSS

https://doi.org/10.5194/acp-2019-1063
Preprint. Discussion started: 3 December 2019

scores of all simulations for domain 03 are small because there are too few data points for evaluation, as mentioned above; slight changes in any of the four factors can cause a large difference in the final scores. However, the CP2k case still has the highest HSS of 0.152, much larger than the maximum and mean HSS of other cases, 0.110 and 0.076, respectively.

3.2.2 Influences of liquid-phase processes on cloud microphysics

Table 3 summarizes the microphysical and radiative properties for all the simulations, including N_c, liquid cloud water path (LCWP), cloud optical depth (τ) and liquid cloud mean effective radius ($\overline{r_e}$) over domain 02 and 03, respectively. Note that only the cloud data in the grid boxes with hydrometeor mixing ratios larger than 0.01 g/kg are included. The equation for τ is:

$$\tau = \frac{3}{2}\frac{1}{\rho_w}\int_0^H \frac{\rho_a q_c(z)}{r_e(z)} dz, \tag{10}$$

where $q_c(z)$ and $r_e(z)$ are mixing ratio and effective radius of cloud droplets at each height (z), respectively; the extinction efficiency is assumed to equal to 2 (appropriate at visible wavelengths) (Grabowski, 2006); H is the cloud top height. Because LCWP= $\int_0^H \rho_a q(z) dz$, the column mean of effective radius is given by

$$\overline{r_e} = \frac{3}{2}\frac{LCWP}{\rho_w \tau}, \tag{11}$$

All sensitivity tests have effects on cloud microphysics in different ways. Changing liquid-phase rain formation processes (i.e. parameterizations of autoconversion and accretion) influences q_c due to their direct effects on the conversion

https://doi.org/10.5194/acp-2019-1063
Preprint. Discussion started: 3 December 2019

rates from cloud droplets to raindrops. On the contrary, dilution caused by the entrainment reduces q_c, and the different mixing mechanisms in the subsequent mixing and evaporation processes determine how many cloud droplets are completely evaporated.

3.2.2.1 Autoconversion

Compared with the control run, the largest differences in all autoconversion cases are 28.2% (28.0%) in LCWP, 18.1% (18.5%) in τ and 4.2% (4.78%) in $\overline{r_e}$ over domain 02 (03) mainly due to one order of magnitude difference of autoconversion rate among different cases (Figures 7a and c). It should be noted that this magnitude of difference is much smaller than that in typical marine boundary layer clouds, which may have over three orders of magnitude difference (Wood, 2005a). Considering that the autoconversion process is indeed sensitive to q_c, there are two reasons responsible for this phenomenon. On the one hand, the temperature of the cloud base over TP region is low; thus the liquid-phase part of the cloud is thin and cloud droplets do not have enough vertical distance to grow; on the other hand, the active ice-phase particles can consume cloud droplets suspended in the supercooled region. Autoconversion is the initial process to produce raindrops, and thus larger autoconversion rate usually brings out larger accretion rate (Figures 7b and d).

https://doi.org/10.5194/acp-2019-1063
Preprint. Discussion started: 3 December 2019

3.2.2.2 Accretion

It is noteworthy that the CP2k scheme has larger differences from the control run than the three autoconversion cases and the Ko13 case, especially for the LCWP-related processes. Compared to the control run, differences of the CP2k case over domain 02 (03) are +64.6% (+51.0%) in LCWP, +36.6% (+28.1%) in τ and +7.9% (+5.6%) in $\overline{r_e}$ while the Ko13 case is much closer to the control run. These large differences are caused by different accretion intensities in different parameterizations. The CP2k case has the weakest accretion intensity compared to the other cases. It should be noted that the weaker accretion process in the CP2k leads to a larger autoconversion rate than that in the control run, different from the argument mentioned above that stronger autoconversion leads to stronger accretion. The larger difference between the CP2k and the control run in domain 02 than in domain 03 is due to the stronger liquid-phase processes in the southeast corner. Details are discussed in the next section.

3.2.2.3 Entrainment-mixing mechanisms

For the entrainment-mixing processes, N_c in the INHOMO run is about 2.6 (4.9) /cm^3 less than the control run, results in (0.9%) 2.4% larger $\overline{r_e}$ over domain 02 (03). The influence of entrainment-mixing processes on $\overline{r_e}$ is larger than the Be68, the LD04, and the Ko13, but smaller than the Bh94 and the CP2k. Different from other sensitivity tests, the influences of entrainment-mixing processes over domain 03 with a higher resolution are more important than domain 02, since the relevant scales involved in this

https://doi.org/10.5194/acp-2019-1063
Preprint. Discussion started: 3 December 2019

process are usually small. The differences between the INHOMO and the control run are similar to the previous studies using the double-moment microphysics scheme (Grabowski and Morrison, 2011; Slawinska et al., 2012). As explained in these studies, entrained air close to saturation is a plausible reason for these small changes (Hoffmann and Feingold, 2019). It is worth noting that our simulations are concerned with a large frontal system with a large cloud cover. The relative humidity of grid boxes experiencing evaporation are mainly larger than 95%.

3.3 Reasons for the precipitation reduction in the CP2k

As mentioned before, compared to other experiments, the CP2k exhibits the largest difference from the control run both for surface precipitation and cloud microphysics. The reasons are discussed in this section.

3.3.1 Detailed microphysical processes in the CP2k

The CP2k experiences an accretion rate that is one to two orders of magnitude smaller than those in the control run and other simulations (Figures 7b and d). The weaker accretion process implies that more liquid cloud water remains suspended in the air and could take part in other microphysical processes such as autoconversion and riming. As shown in Figures 7a and c, the autoconversion rate in the CP2k is much larger than that in the control run; the difference is close to the value that applying different autoconversion schemes directly can cause. Combining two dominant liquid-

https://doi.org/10.5194/acp-2019-1063
Preprint. Discussion started: 3 December 2019

phase rain formation processes (autoconversion and accretion), less cloud water is depleted in the CP2k; as a result, the mean value of LCWP is over 50.0% larger than that of the control run, as shown in Table 3. Figure 8 shows the vertical profiles of the mean differences of the dominant conversion process rates between the CP2k and the control run (CP2k-Control) over the two regions in domain 02 and during the two precipitation peak periods in domain 03. Similar to Figure 7, the CP2k has a much smaller accretion rate and larger autoconversion rate. Despite the larger autoconversion rate, many cloud droplets are suspended above the 0 ℃ isotherm, beneficial for riming of cloud droplets onto snow or graupel particles (RIM-s + RIM-g). Due to the larger riming rate, more ice-phase particles melt to more raindrops below the 0 ℃ isotherm (MELT). Note that the smaller melting rate near 6 ~ 6.5 km in the CP2k over domain 03 is because of the lower melting level in CP2k than in the control run. Table 3 shows that τ in the CP2k is larger, which means more solar radiation is reflected to the upper atmosphere and less short-wave radiation reaches the ground (219.6 W/m^2 in the CP2k vs 226.5 W/m^2 in the control run). Such a difference in radiation results in a lower temperature in the CP2k in the low atmosphere than in the control run. Therefore, the melting level is lower in the CP2k.

The source of surface precipitation includes both the liquid-phase (mainly ACCR-r) and the ice-phase (MELT). During the first precipitation peak period in domain 03, despite of the smaller accretion rate in the CP2k than that in the control run, more riming leads to more melting. The combination of weaker accretion and more melting in the

https://doi.org/10.5194/acp-2019-1063
Preprint. Discussion started: 3 December 2019

Atmospheric Chemistry and Physics Discussions

CP2k offset each other, and hence the precipitation from the CP2k and the control run is very close in this period (Figure 6b). A similar chain of events also occurs in domain 02 except for the southeastern corner (Figures 2b and 5d). However, in the control run, due to relatively low concentration of ice particles during the second peak period in domain 03, the liquid-phase processes, in particular accretion, become relatively more important (Figure 4h); for the southeastern corner of domain 02, the large mixing ratio of cloud droplets even causes the accretion rate to exceed the melting rate (Figure 4d). Surface precipitation is overestimated in the control run compared with the observations, as discussed in Section 3.2.1. In the CP2k, the accretion is suppressed which appears to alleviate the overestimation of precipitation. Therefore, the total surface precipitation in the CP2k is smaller than that in the control run over the southeastern corner in domain 02 and during the second peak period in domain 03, which is closer to observations.

3.3.2 Detailed analysis of the CP2k parameterization

The large differences in cloud microphysics and precipitation between the CP2k and other cases can be explained based on the different equations for autoconversion and accretion (Eq. 2, 6 and 7). The different equations for the autoconversion and accretion can be separated into two basic methods as mentioned in Wood (2005a): the first one integrates the stochastic collection equation for a wide range of drop size distributions and then uses a simple power-law fit, such as the KK scheme in the control run. The second method simplifies the collection kernel and parameterizes the

https://doi.org/10.5194/acp-2019-1063
Preprint. Discussion started: 3 December 2019

Atmospheric Chemistry and Physics Discussions

autoconversion and accretion processes, such as the parametrization of the autoconversion rate in LD04 and accretion rate in the CP2k. Autoconversion schemes commonly use one of these basic methods. However, the accretion schemes used in most of the microphysical schemes are based on the first method, and previous studies largely compare these accretion schemes (Wood, 2005a; Hill et al., 2015). As shown above and also below, the CP2k accretion rate parameterization is unique and appears superior to other parameterizations, but this parameterization is only used in a few microphysics schemes (e.g. WDM6 scheme in WRF, Lim and Hong, 2010).

Figure 9 compares the accretion rate calculated as a function of raindrop radius for all the accretion schemes under the conditions of $q_c = 1$ g/kg, $R_c = 10$ μm, $N_r = 4000$ /m^3. It is obvious that the three schemes result in different relationships for the accretion rate. Considering the power-law form in the formula from the first method, i.e., the KK scheme in the control run and the Ko13 scheme, accretion rate is linearly related to raindrop radius in the logarithmic space. However, the CP2k accretion rate has an inflection point at 50 μm due to the piecewise function in Eq. 6. Under the condition of adequate cloud water, the accretion process in the KK or the Ko13 scheme only depends on rain water mixing ratio. However, in the CP2k, if the raindrop radius is less than 50 μm, the accretion rate is very small. As shown in Figure 9, the accretion rate in the KK or the Ko13 scheme is always larger than in the CP2k when the raindrop radius is smaller than 2000 μm. The difference between the CP2k and the other two schemes increases with decreasing raindrop radius; especially when the raindrop radius is

https://doi.org/10.5194/acp-2019-1063
Preprint. Discussion started: 3 December 2019

smaller than 50 μm, with the maximum difference being more than two orders of magnitude. Therefore, the probability density distributions (PDFs) of raindrop radius are important for the difference between different accretion rate schemes. Figure 10 shows the probability density distributions (PDFs) of raindrop radius used in the accretion process in the three schemes. All raindrops are smaller than 10^3 μm. The PDFs have peaks of ~30, ~30 and ~25 μm in the control run, the Ko13 and the CP2k, respectively, and the cumulative PDF shows that the raindrops with radius smaller than 50 μm have frequencies of 58.8%, 53.8%, and 46.0%, respectively. The drop size distributions from both aircraft observations and bin models confirm that a large proportion of liquid droplets have radii larger than 25 μm but smaller than 50 μm (Wood, 2005b; Morrison and Grabowski, 2007). Such large percentage of small raindrops makes the accretion rate and precipitation in the CP2k quite different from that in other schemes (Figure 9). Furthermore, there is a positive feedback mechanism, since accretion increases q_r and accretion rate is positively correlated with q_r. The overestimation of the accretion rate in the control run hence feeds back on itself. This is the reason why the precipitation and accretion rate differences between the control run and the CP2k are so different over the southeastern corner in domain 02 and during the second peak period in domain 03.

Previous studies have shown that, to initiate liquid phase precipitation, the cloud effective radius needs to reach about 14 μm (Rosenfeld et al., 2019). A closer look on the cloud droplet size distributions is hence informative to understand the differences in precipitation behavior between the CP2k and the other experiments. Figure 11 shows the liquid-phase precipitation rate as a function of cloud droplet effective radius. The liquid-phase precipitation rate is estimated as the product of total precipitation and the ratio of liquid-phase process rates (autoconversion + accretion) and ice-phase process rates (melting from snow + graupel). The liquid-phase precipitation rate exceeds 2 mm/day when the cloud effective radius is 9 μm in the control run and the Ko13. In the CP2k, it is not until the cloud effective radius reaches about 15 μm, that the precipitation rate exceeds 2 mm/day. The contribution from autoconversion is close to 0 in the control run, which could be due to the consumption of cloud droplets by accretion after droplets reach 9 μm. The value of 9 μm, is much smaller than 14 μm needed to initiate liquid-phase precipitation, often suggested by observational studies. On the contrary, there is a significant increase in liquid-phase precipitation rate from the autoconversion process in the CP2k at 15 μm and then the accretion process begins to efficiently produce liquid-phase precipitation. Therefore, the improvement in the CP2k surface precipitation compared to the control, appears to occur for the right reasons.

4. Summary and conclusions

In this paper, a typical summer plateau precipitation event over the Tibetan Plateau is simulated using the WRFv3.8.1 model with the Morrison double-moment scheme. The control run reproduces the primary spatial distribution and temporal evolution of precipitation rate. However, the precipitation in the coarse resolution domain is about

https://doi.org/10.5194/acp-2019-1063
Preprint. Discussion started: 3 December 2019

twice of the observed value, similar to previous studies which claimed that the overprediction was due to low resolution or inaccurate large-scale forcing. The precipitation in the higher resolution domain is more consistent with the observations, but still, the precipitation during the second precipitation peak period in this domain is overpredicted.

To understand the roles of liquid-phase microphysical processes in the overprediction of precipitation, sensitivity tests are carried out by introducing different parameterizations of liquid-phase processes into the Morrison double-moment scheme, including three autoconversion parameterizations (Be68, Bh94 and LD04), two accretion parameterizations (CP2k and Ko13), and one entrainment-mixing parameterization (INHOMO).

The overprediction of precipitation is significantly reduced in both the low- and high-resolution domains in the experiment using the Cohard and Pinty (2000) accretion scheme (CP2k). The Heidke skill scores with the CP2k also show better results compared to other cases. Furthermore, each simulation is further divided into two parts: one with dominant ice-phase processes, the other with dominant liquid-phase processes. The simulations have the largest differences when the liquid-phase processes dominate, and the improvement in the CP2k experiment is more pronounced in this case. When the ice-phase processes are important, all the simulations are equivalent, including the CP2k. There are several reasons for this behavior. The accretion rate is smaller in the CP2k experiment than that in the control run, which suppresses precipitation due to

https://doi.org/10.5194/acp-2019-1063
Preprint. Discussion started: 3 December 2019

liquid-phase processes. Due to weaker accretion, more cloud droplets remain suspended in the atmosphere and are available for riming onto snow and graupel. Precipitation due to melting from snow and graupel is then enhanced. The combination of the weaker accretion and stronger melting in the CP2k offset each other. That is the reason why the precipitation does not change much in the CP2k when ice-phase processes dominate. When the ice-phase processes are relatively weak, the precipitation from the enhanced riming and melting processes cannot compensate the loss of precipitation due to the suppression of accretion. Therefore, the precipitation rate is smaller in the CP2k than in the control run.

To understand the physical reasons for the improved performance of the CP2k, the equations for parameterizing the accretion rate in the CP2k, the KK and the Ko13 are compared directly. The accretion rate in the CP2k is always smaller than in the KK or Ko13 scheme when the raindrop radius is smaller than 2000 µm. Furthermore, the difference increases with decreasing raindrop radius and can amount to more than two orders of magnitude when the raindrop radius is smaller than 50 µm. The PDFs of raindrop radii have their peaks around 30 µm. Around 50% of raindrops have radius less than 50 µm. This is the reason why the CP2k suppresses accretion and liquid-phase precipitation compared to the other two schemes. Further insight in the reasons for different behavior in the CP2k compared to the other schemes is provided through the relation of cloud droplet size and liquid phase precipitation rates. It is often claimed that, to initiate liquid-phase precipitation, cloud effective radius needs to reach 14 µm.

https://doi.org/10.5194/acp-2019-1063
Preprint. Discussion started: 3 December 2019

When the cloud effective radius is 9 μm in the control run and the Ko13, the liquid-phase precipitation rate already exceeds 2 mm/day however; In the CP2k, on the other hand, liquid phase precipitation does not start until the effective radius reaches about 15 μm, which is more consistent with observations.

Author contributions. CL and XX designed the experiments. XX carried out the experiments and conducted the data analysis with contributions from all coauthors. KVW developed the model code. XX prepared the paper with help from CL, YL, WG, YW, YC, SL, and KVW.

Competing interests. The authors declare that they have no conflict of interest.

Acknowledgements. The authors thank the Amy Solomon for providing the microphysics scheme, Yinzhao Ma and Yang Hong for providing the precipitation data. This research is supported by the National Key Research and Development Program of China (2017YFA0604000), the Natural Science Foundation of Jiangsu Province (BK20160041), the National Natural Science Foundation of China (41822504, 91537108), the Qinglan Project (R2018Q05), and the Six Talent Peak Project in Jiangsu (2015-JY-011). Liu is supported by the U.S. Department of Energy Office of Science Biological and Environmental Research as part of the Atmospheric Systems Research (ASR) Program and Solar Energy and Technology Office (SETO). Brookhaven

https://doi.org/10.5194/acp-2019-1063
Preprint. Discussion started: 3 December 2019

National Laboratory is operated by Battelle for the U.S. Department of Energy under Contract DE-SC00112704.

Appendix A: Symbol List

N_c: number concentration of cloud droplets

q_c: mixing ratio of cloud droplet

N_r: number concentration of raindrops

q_r: mixing ratio of raindrops

N_i: number concentration of ice crystals

q_i: mixing ratio of ice crystals

N_s: number concentration of snow particles

q_s: mixing ratio of snow particles

N_g: number concentration of graupel particles

q_g: mixing ratio of graupel particles

R_{accr}: conversion rate of accretion process

R_{auto}: conversion rate of autoconversion process

ρ_a: air density

ε: dispersion

ρ_W: water density

λ: slope parameter

N_{c0}: number concentration of cloud water droplets before evaporation process

https://doi.org/10.5194/acp-2019-1063
Preprint. Discussion started: 3 December 2019

Atmospheric Chemistry and Physics Discussions
Open Access
EGU

q_{c0}: mixing ratio of cloud water droplets before evaporation process

p_t: the threshold value of precipitation in the Heidke skill score

p_s: value of precipitation from simulations in the Heidke skill score

p_o: value of precipitation from observation in the Heidke skill score

τ: cloud optical depth

$\overline{r_e}$: averaged effective radius of cloud water droplets

LCWP: liquid cloud water path

EVAP-r: evaporation of raindrops

ACCR-r: accretion of cloud liquid water by rain

AUTO-r: autoconversion from cloud droplets to raindrops

MELT: melting from snow or graupel particles to raindrops

AUTO-s: autoconversion of cloud ice to snow

ACCR-s: accretion of cloud ice by snow

RIM-s: accretion of cloud droplets by snow particle

RIM-g: accretion of cloud droplets by graupel particle

https://doi.org/10.5194/acp-2019-1063
Preprint. Discussion started: 3 December 2019

Atmospheric Chemistry and Physics Discussions

Reference:

Barnston, A. G.: Correspondence among the correlation, RMSE, and Heidke forecast verification measures; refinement of the Heidke score, Weather and Forecasting, 7, 699-709, 1992.

Chen, B., Hu, Z., Liu, L., and Zhang, G.: Raindrop Size Distribution Measurements at 4,500 m on the Tibetan Plateau During TIPEX-III, Journal of Geophysical Research: Atmospheres, 122, 11,092-011,106, 2017a.

Chen, J., Wu, X., Yin, Y., Huang, Q., and Xiao, H.: Characteristics of Cloud Systems over the Tibetan Plateau and East China during Boreal Summer, Journal of Climate, 30, 3117-3137, 2017b.

Chosson, F., Brenguier, J.-L., and Schüller, L.: Entrainment-mixing and radiative transfer simulation in boundary layer clouds, Journal of the atmospheric sciences, 64, 2670-2682, 2007.

Cohard, J. M., and Pinty, J. P.: A comprehensive two-moment warm microphysical bulk scheme. I: Description and tests, Quarterly Journal of the Royal Meteorological Society, 126, 1815-1842, 2000.

Cooper, W. A., Lasher-Trapp, S. G., and Blyth, A. M.: The Influence of Entrainment and Mixing on the Initial Formation of Rain in a Warm Cumulus Cloud, Journal of the Atmospheric Sciences, 70, 1727-1743, 10.1175/jas-d-12-0128.1, 2013.

Ding, Y., Zhang, Y., Ma, Q., and Hu, G.: Analysis of the large-scale circulation features and synoptic systems in East Asia during the intensive observation period of

https://doi.org/10.5194/acp-2019-1063
Preprint. Discussion started: 3 December 2019

GAME/HUBEX, Journal of the Meteorological Society of Japan. Ser. II, 79, 277-300, 2001.

Fan, J., Rosenfeld, D., Zhang, Y., Giangrande, S. E., Li, Z., Machado, L. A. T., Martin, S. T., Yang, Y., Wang, J., Artaxo, P., Barbosa, H. M. J., Braga, R. C., Comstock, J. M., Feng, Z., Gao, W., Gomes, H. B., Mei, F., Pohlker, C., Pohlker, M. L., Poschl, U., and de Souza, R. A. F.: Substantial convection and precipitation enhancements by ultrafine aerosol particles, Science, 359, 411-418, 10.1126/science.aan8461, 2018.

Flohn, H.: Large-scale aspects of the "summer monsoon" in South and East Asia, Journal of the Meteorological Society of Japan. Ser. II, 35, 180-186, 1957.

Fu, Y., Li, H., and Zi, Y.: Case study of precipitation cloud structure viewed by TRMM satellite in a valley of the Tibetan Plateau, Plateau Meteorol, 26, 98-106, 2007.

Fujinami, H., and Yasunari, T.: The seasonal and intraseasonal variability of diurnal cloud activity over the Tibetan Plateau, Journal of the Meteorological Society of Japan. Ser. II, 79, 1207-1227, 2001.

Gao, W., Sui, C. H., Fan, J., Hu, Z., and Zhong, L.: A study of cloud microphysics and precipitation over the Tibetan Plateau by radar observations and cloud-resolving model simulations, Journal of Geophysical Research: Atmospheres, 121, 13,735-713,752, 2016.

Gao, W., Liu, L., Li, J., and Lu, C.: The Microphysical Properties of Convective Precipitation Over the Tibetan Plateau by a Subkilometer Resolution Cloud-

https://doi.org/10.5194/acp-2019-1063
Preprint. Discussion started: 3 December 2019

Resolving Simulation, Journal of Geophysical Research: Atmospheres, 123, 3212-3227, 2018.

Gerken, T., Babel, W., Sun, F., Herzog, M., Ma, Y., Foken, T., and Graf, H.-F.: Uncertainty in atmospheric profiles and its impact on modeled convection development at Nam Co Lake, Tibetan Plateau, Journal of Geophysical Research: Atmospheres, 118, 12,317-312,331, 10.1002/2013jd020647, 2013.

Gettelman, A., Morrison, H., Terai, C. R., and Wood, R.: Microphysical process rates and global aerosol–cloud interactions, Atmospheric Chemistry and Physics, 13, 9855-9867, 10.5194/acp-13-9855-2013, 2013.

Grabowski, W. W.: Indirect impact of atmospheric aerosols in idealized simulations of convective–radiative quasi equilibrium, Journal of climate, 19, 4664-4682, 2006.

Grabowski, W. W., and Morrison, H.: Indirect Impact of Atmospheric Aerosols in Idealized Simulations of Convective–Radiative Quasi Equilibrium. Part II: Double-Moment Microphysics, Journal of Climate, 24, 1897-1912, 10.1175/2010jcli3647.1, 2011.

Hahn, D. G., and Manabe, S.: The role of mountains in the south Asian monsoon circulation, Journal of the Atmospheric Sciences, 32, 1515-1541, 1975.

Hill, A. A., Shipway, B. J., and Boutle, I. A.: How sensitive are aerosol-precipitation interactions to the warm rain representation?, Journal of Advances in Modeling Earth Systems, 7, 987-1004, 10.1002/2014ms000422, 2015.

Hoffmann, F., and Feingold, G.: Entrainment and Mixing in Stratocumulus: Effects of

https://doi.org/10.5194/acp-2019-1063
Preprint. Discussion started: 3 December 2019

Atmospheric Chemistry and Physics Discussions

a New Explicit Subgrid-Scale Scheme for Large-Eddy Simulations with Particle-Based Microphysics, Journal of the Atmospheric Sciences, 76, 1955-1973, 10.1175/jas-d-18-0318.1, 2019.

Hsu, H. H., and Liu, X.: Relationship between the Tibetan Plateau heating and East Asian summer monsoon rainfall, Geophysical Research Letters, 30, 2003.

Jing, X., and Suzuki, K.: The Impact of Process-Based Warm Rain Constraints on the Aerosol Indirect Effect, Geophysical Research Letters, 45, 10,729-710,737, 2018.

Khairoutdinov, M., and Kogan, Y.: A new cloud physics parameterization in a large-eddy simulation model of marine stratocumulus, Monthly weather review, 128, 229-243, 2000.

Kogan, Y.: A cumulus cloud microphysics parameterization for cloud-resolving models, Journal of the Atmospheric Sciences, 70, 1423-1436, 2013.

Kurosaki, Y., and Kimura, F.: Relationship between topography and daytime cloud activity around Tibetan Plateau, Journal of the Meteorological Society of Japan. Ser. II, 80, 1339-1355, 2002.

Lasher-Trapp, S. G., Cooper, W. A., and Blyth, A. M.: Broadening of droplet size distributions from entrainment and mixing in a cumulus cloud, Quarterly Journal of the Royal Meteorological Society, 131, 195-220, 10.1256/qj.03.199, 2005.

Li, J., You, L.-g., Hu, Z.-j., Tu, D.-b., and Li, L.-g.: Analysis on raindrop-size distribution characteristics of Maqu region in upper reach of Yellow River, Plateau Meteorology, 25, 942-949, 2006.

https://doi.org/10.5194/acp-2019-1063
Preprint. Discussion started: 3 December 2019

Li, Y., Wang, Y., Song, Y., Hu, L., Gao, S., and Rong, F.: Characteristics of Summer Convective Systems Initiated over the Tibetan Plateau. Part I: Origin, Track, Development, and Precipitation, Journal of Applied Meteorology and Climatology, 47, 2679-2695, 10.1175/2008jamc1695.1, 2008.

Lim, K.-S. S., and Hong, S.-Y.: Development of an Effective Double-Moment Cloud Microphysics Scheme with Prognostic Cloud Condensation Nuclei (CCN) for Weather and Climate Models, Monthly Weather Review, 138, 1587-1612, 10.1175/2009mwr2968.1, 2010.

Liu, Y., and Daum, P. H.: Parameterization of the autoconversion process. Part I: Analytical formulation of the Kessler-type parameterizations, Journal of the atmospheric sciences, 61, 1539-1548, 2004.

Liu, Y.: Size truncation effect, threshold behavior, and a new type of autoconversion parameterization, Geophysical Research Letters, 32, 10.1029/2005gl022636, 2005.

Lu, C., Liu, Y., Niu, S., Krueger, S., and Wagner, T.: Exploring parameterization for turbulent entrainment-mixing processes in clouds, Journal of Geophysical Research: Atmospheres, 118, 185-194, 10.1029/2012jd018464, 2013.

Luo, H., and Yanai, M.: The large-scale circulation and heat sources over the Tibetan Plateau and surrounding areas during the early summer of 1979. Part I: Precipitation and kinematic analyses, Monthly Weather Review, 111, 922-944, 1983.

Luo, H., and Yanai, M.: The large-scale circulation and heat sources over the Tibetan

https://doi.org/10.5194/acp-2019-1063
Preprint. Discussion started: 3 December 2019

Plateau and surrounding areas during the early summer of 1979. Part II: Heat and moisture budgets, Monthly Weather Review, 112, 966-989, 1984.

Ma, Y., Hong, Y., Chen, Y., Yang, Y., Tang, G., Yao, Y., Long, D., Li, C., Han, Z., and Liu, R.: Performance of Optimally Merged Multisatellite Precipitation Products Using the Dynamic Bayesian Model Averaging Scheme Over the Tibetan Plateau, Journal of Geophysical Research: Atmospheres, 123, 814-834, 10.1002/2017jd026648, 2018.

Maussion, F., Scherer, D., Finkelnburg, R., Richters, J., Yang, W., and Yao, T.: WRF simulation of a precipitation event over the Tibetan Plateau, China – an assessment using remote sensing and ground observations, Hydrology and Earth System Sciences, 15, 1795-1817, 10.5194/hess-15-1795-2011, 2011.

Michibata, T., and Takemura, T.: Evaluation of autoconversion schemes in a single model framework with satellite observations, Journal of Geophysical Research: Atmospheres, 120, 9570-9590, 2015.

Molnar, P., Boos, W. R., and Battisti, D. S.: Orographic controls on climate and paleoclimate of Asia: thermal and mechanical roles for the Tibetan Plateau, Annual Review of Earth and Planetary Sciences, 38, 77-102, 2010.

Morrison, H., Curry, J., and Khvorostyanov, V.: A new double-moment microphysics parameterization for application in cloud and climate models. Part I: Description, Journal of the atmospheric sciences, 62, 1665-1677, 2005.

Morrison, H., and Grabowski, W. W.: Comparison of Bulk and Bin Warm-Rain

https://doi.org/10.5194/acp-2019-1063
Preprint. Discussion started: 3 December 2019

Atmospheric Chemistry and Physics Discussions

Microphysics Models Using a Kinematic Framework, Journal of the Atmospheric Sciences, 64, 2839-2861, 10.1175/jas3980, 2007.

Morrison, H., and Grabowski, W. W.: Modeling Supersaturation and Subgrid-Scale Mixing with Two-Moment Bulk Warm Microphysics, Journal of the Atmospheric Sciences, 65, 792-812, 10.1175/2007jas2374.1, 2008.

Nitta, T.: Observational study of heat sources over the eastern Tibetan Plateau during the summer monsoon, Journal of the Meteorological Society of Japan. Ser. II, 61, 590-605, 1983.

Porcù, F., D'Adderio, L. P., Prodi, F., and Caracciolo, C.: Rain drop size distribution over the Tibetan Plateau, Atmospheric research, 150, 21-30, 2014.

Rosenfeld, D., Zhu, Y., Wang, M., Zheng, Y., Goren, T., and Yu, S.: Aerosol-driven droplet concentrations dominate coverage and water of oceanic low-level clouds, Science, 363, eaav0566, 2019.

Sato, T., Yoshikane, T., Satoh, M., MIURA, H., and Fujinami, H.: Resolution dependency of the diurnal cycle of convective clouds over the Tibetan Plateau in a mesoscale model, Journal of the Meteorological Society of Japan. Ser. II, 86, 17-31, 2008.

Shen, R., Reiter, E. R., and Bresch, J. F.: Some aspects of the effects of sensible heating on the development of summer weather systems over the Tibetan Plateau, Journal of the atmospheric sciences, 43, 2241-2260, 1986.

Slawinska, J., Grabowski, W. W., Pawlowska, H., and Wyszogrodzki, A. A.: Optical

Properties of Shallow Convective Clouds Diagnosed from a Bulk-Microphysics Large-Eddy Simulation, Journal of Climate, 21, 1639-1647, 10.1175/2007jcli1820.1, 2008.

Slawinska, J., Grabowski, W. W., Pawlowska, H., and Morrison, H.: Droplet Activation and Mixing in Large-Eddy Simulation of a Shallow Cumulus Field, Journal of the Atmospheric Sciences, 69, 444-462, 10.1175/jas-d-11-054.1, 2012.

Tang, J., Guo, X., and Chang, Y.: A numerical investigation on microphysical properties of clouds and precipitation over the Tibetan Plateau in summer 2014, Journal of Meteorological Research, 33, 463-477, 2019.

Ueda, H., and Yasunari, T.: Role of warming over the Tibetan Plateau in early onset of the summer monsoon over the Bay of Bengal and the South China Sea, Journal of the Meteorological Society of Japan. Ser. II, 76, 1-12, 1998.

Ueda, H., Kamahori, H., and Yamazaki, N.: Seasonal contrasting features of heat and moisture budgets between the eastern and western Tibetan Plateau during the GAME IOP, Journal of climate, 16, 2309-2324, 2003.

Wang, B., Bao, Q., Hoskins, B., Wu, G., and Liu, Y.: Tibetan Plateau warming and precipitation changes in East Asia, Geophysical Research Letters, 35, 2008.

Wang, M., Ghan, S., Liu, X., L'Ecuyer, T. S., Zhang, K., Morrison, H., Ovchinnikov, M., Easter, R., Marchand, R., Chand, D., Qian, Y., and Penner, J. E.: Constraining cloud lifetime effects of aerosols using A-Train satellite observations, Geophysical Research Letters, 39, 10.1029/2012gl052204, 2012.

https://doi.org/10.5194/acp-2019-1063
Preprint. Discussion started: 3 December 2019

Wang, W., Kuo, Y.-H., and Warner, T. T.: A diabatically driven mesoscale vortex in the lee of the Tibetan Plateau, Monthly weather review, 121, 2542-2561, 1993.

Wang, Y., Wan, Q., Meng, W., Liao, F., Tan, H., and Zhang, R.: Long-term impacts of aerosols on precipitation and lightning over the Pearl River Delta megacity area in China, Atmospheric Chemistry and Physics, 11, 12421-12436, 2011.

Wang, Y., Niu, S., Lu, C., Liu, Y., Chen, J., and Yang, W.: An Observational Study on Cloud Spectral Width in North China, Atmosphere, 10, 109, 10.3390/atmos10030109, 2019.

Wood, R.: Drizzle in stratiform boundary layer clouds. Part II: Microphysical aspects, Journal of the atmospheric sciences, 62, 3034-3050, 2005a.

Wood, R.: Drizzle in stratiform boundary layer clouds. Part I: Vertical and horizontal structure, Journal of the Atmospheric Sciences, 62, 3011-3033, 2005b.

Wu, G. X., and Chen, S. J.: The effect of mechanical forcing on the formation of a mesoscale vortex, Quarterly Journal of the Royal Meteorological Society, 111, 1049-1070, 1985.

Wu, Y., and Liu, L.: Statistical characteristics of raindrop size distribution in the Tibetan Plateau and southern China, Advances in Atmospheric Sciences, 34, 727-736, 2017.

Xie, X., and Liu, X.: Effects of spectral dispersion on clouds and precipitation in mesoscale convective systems, Journal of Geophysical Research: Atmospheres, 116, 2011.

https://doi.org/10.5194/acp-2019-1063
Preprint. Discussion started: 3 December 2019

Atmospheric Chemistry and Physics Discussions
Open Access

Xie, X., Liu, X., Peng, Y., Wang, Y., Yue, Z., and Li, X.: Numerical simulation of clouds and precipitation depending on different relationships between aerosol and cloud droplet spectral dispersion, Tellus Series B-Chemical and Physical Meteorology, 65, 10.3402/tellusb.v65i0.19054, 2013.

Xu, J., Zhang, B., Wang, M., and Wang, H.: Diurnal variation of summer precipitation over the Tibetan Plateau: a cloud-resolving simulation, Annales Geophysicae, 2012, 1575-1586,

Yanai, M., Li, C., and Song, Z.: Seasonal heating of the Tibetan Plateau and its effects on the evolution of the Asian summer monsoon, Journal of the Meteorological Society of Japan. Ser. II, 70, 319-351, 1992.

Yanai, M., and Li, C.: Mechanism of heating and the boundary layer over the Tibetan Plateau, Monthly Weather Review, 122, 305-323, 1994.

Yang, K., Wu, H., Qin, J., Lin, C., Tang, W., and Chen, Y.: Recent climate changes over the Tibetan Plateau and their impacts on energy and water cycle: A review, Global and Planetary Change, 112, 79-91, 2014.

Ye, D.: Some characteristics of the summer circulation over the Qinghai-Xizang (Tibet) Plateau and its neighborhood, Bulletin of the American Meteorological Society, 62, 14-19, 1981.

Yeh, T. C.: The circulation of the high troposphere over China in the winter of 1945–46, Tellus, 2, 173-183, 1950.

Yin, Z.-Y., Zhang, X., Liu, X., Colella, M., and Chen, X.: An assessment of the biases

https://doi.org/10.5194/acp-2019-1063
Preprint. Discussion started: 3 December 2019

Atmospheric Chemistry and Physics Discussions

of satellite rainfall estimates over the Tibetan Plateau and correction methods based on topographic analysis, Journal of Hydrometeorology, 9, 301-326, 2008.

Zhao, C., Tie, X., Brasseur, G., Noone, K. J., Nakajima, T., Zhang, Q., Zhang, R., Huang, M., Duan, Y., and Li, G.: Aircraft measurements of cloud droplet spectral dispersion and implications for indirect aerosol radiative forcing, Geophysical research letters, 33, 2006.

Zhao, C., Liu, L., Wang, Q., Qiu, Y., Wang, Y., and Wu, X.: MMCR-based characteristic properties of non-precipitating cloud liquid droplets at Naqu site over Tibetan Plateau in July 2014, Atmospheric Research, 190, 68-76, 10.1016/j.atmosres.2017.02.002, 2017.

Zhou, X., Bei, N., Liu, H., Cao, J., Xing, L., Lei, W., Molina, L. T., and Li, G.: Aerosol effects on the development of cumulus clouds over the Tibetan Plateau, Atmospheric Chemistry and Physics, 17, 7423-7434, 10.5194/acp-17-7423-2017, 2017.

https://doi.org/10.5194/acp-2019-1063
Preprint. Discussion started: 3 December 2019

Caption List:

Table 1. Contingency table used to calculate the Heidke skill score (HSS). The elements *a-d* represent the numbers of "hits", "false alarms", "misses" and "correct negatives", respectively. p_t is the threshold value of precipitation in observation and simulations, p_s is the value from simulations and p_o is the value from observations.

Table 2. The values of four elements *a-d* and Heidke skill score (HSS) for all simulations over domain 02 and domain 03 (d02/d03), respectively.

Table 3. The mean number concentration N_c (/cm^3), effective radius $\overline{r_e}$ (μm) of cloud droplets, area-averaged liquid cloud water path LCWP (g/m^2), cloud optical depth τ over domain 02 and 03 (d02/d03) of the control run, Be68, Bh94, LD04 (different autoconversion schemes), CP2k, Ko13 (different accretion schemes) and INHOMO run (different mixing mechanism).

Figure 1. Geographic locations of the three domains used in the numerical simulation.

Figure 2. Spatial distributions of 48 h accumulated precipitation (mm) during 0000 UTC 22 July to 0000 UTC 24 July 2014 from the observations and the control run over domain 02 (a, b) and domain 03 (c, d).

Figure 3. Time series of area-averaged hourly precipitation rate (mm/h) during 0000 UTC 22 July to 0000 UTC 24 July 2014 over (a) domain 02 and (b) domain 03 from the observations and the control run.

Figure 4. Mean vertical profiles of mixing ratios (g/kg) of cloud droplets (q_c), raindrops(q_r), ice particles(q_i), snow particles (q_s), graupel particles(q_g) and their

https://doi.org/10.5194/acp-2019-1063
Preprint. Discussion started: 3 December 2019

primary microphysical processes in the control run (a, b) averaged from 48 h over domain 02 except southeastern corner, (c, d)averaged from 48 h at southeastern corner over domain 02, averaged during two precipitation peaks (e, f) 0700-1200 UTC 22 July 2014 and (g, h) 0700-1200 UTC 23 July 2014 over domain 03. The purple dot-dash lines denote the mean height of 0 °C isotherm.

Figure 5. Spatial distributions of 48 h accumulated precipitation (mm) during 0000 UTC 22 July to 0000 UTC 24 July 2014 from observations and all sensitivity simulations over (a-f) domain 02 and (g-l) domain 03.

Figure 6. Time series of area-averaged hourly precipitation rate (mm/h) during 0000 UTC 22 July to 0000 UTC 24 July 2014 over (a) domain 02 and (b) domain 03 from the observations and all simulations.

Figure 7. The time series of area-averaged autoconversion rate and accretion rate over (a, b) domain 02 and (c, d) domain 03 for all simulations, respectively.

Figure 8. Differences of mean vertical profiles of the dominated microphysical processes conversion rates between the CP2k and the control run (CP2k-Control) from (a) domain 02 except southeastern corner, (b) the southeastern corner of domain 02, and during the two precipitation peak periods (c) 0700-1200 UTC 22 July and (d) 0700-1200 UTC 23 July over domain 03. The purple dot-dash lines denote the mean height of 0 °C isotherm.

https://doi.org/10.5194/acp-2019-1063
Preprint. Discussion started: 3 December 2019

Figure 9. The accretion rate as a function of raindrop radius with fixed cloud mixing ratio q_c = 1 g/kg, the radius of cloud droplet R_c = 10 μm, number concentration of raindrops N_r = 4000 /m^3 for the three accretion schemes.

Figure 10. Probability distribution function (PDF) and cumulative PDF of raindrop radius involved in the accretion process for (a) the control run, (b) the CP2k, and (c) the Ko13. The purple line denotes the radius of raindrop equal to 50 μm.

Figure 11. Dependence of warm rain intensity on cloud effective radius from the control run and the CP2k during 0000 UTC 22 July to 0000 UTC 24 July 2014 over domain 03.

https://doi.org/10.5194/acp-2019-1063
Preprint. Discussion started: 3 December 2019

Table 1. Contingency table used to calculate the Heidke skill score (HSS). The elements *a*-*d* represent the numbers of "hits", "false alarms", "misses" and "correct negatives", respectively. p_t is the threshold value of precipitation in observation and simulations, p_s is the value from simulations and p_o is the value from observations.

	Observation $p_o > p_t$	Observation $p_o \le p_t$
Simulation $p_s > p_t$	*a*	*b*
Simulation $p_s \le p_t$	*c*	*d*

https://doi.org/10.5194/acp-2019-1063
Preprint. Discussion started: 3 December 2019

Atmospheric Chemistry and Physics Discussions

Table 2. The values of four elements *a-d* and Heidke skill score (HSS) for all simulations over domain 02 and domain 03 (d02/d03), respectively.

	a	*b*	*c*	*d*	HSS
control	2636/304	1224/148	773/76	2231/48	0.419/0.049
autoconversion					
Be68	2645/309	1261/142	764/71	2194/54	0.411/0.097
Bh94	2533/306	1148/138	876/74	2307/58	0.411/0.110
LD04	2628/313	1264/154	781/67	2191/42	0.405/0.043
accretion					
CP2k	2583/304	1063/129	632/76	2586/67	0.508/0.152
K013	2620/303	1223/146	770/77	2251/50	0.420/0.057
mixing mechanism					
INHOMO	2656/308	1124/141	753/72	2214/55	0.420/0.100

https://doi.org/10.5194/acp-2019-1063
Preprint. Discussion started: 3 December 2019

Atmospheric Chemistry and Physics Discussions
Open Access
EGU

Table 3. The mean number concentration N_c (/cm^3), effective radius $\overline{r_e}$ (μm) of cloud droplets, area-averaged liquid cloud water path LCWP (g/m^2), cloud optical depth τ over domain 02 and 03 (d02/d03) of the control run, Be68, Bh94, LD04 (different autoconversion schemes), CP2k, Ko13 (different accretion schemes) and INHOMO run (different mixing mechanism).

	N_c(/cm^3)	LCWP(g/m^2)	τ	$\overline{r_e}$ (μm)
control	71.5/91.2	73.5/66.8	11.9/11.1	6.97/6.77
autoconversion				
Be68	71.3/91.6	63.4/59.4	10.8/10.6	6.84/6.74
Bh94	72.3/91.9	81.3/76.1	12.7/12.6	7.13/7.01
LD04	71.6/91.3	63.8/60.9	10.8/10.6	6.85/6.69
accretion				
CP2k	72.4/90.1	121.0/97.0	16.3/14.3	7.52/7.15
Ko13	71.5/91.0	74.4/64.4	11.6/10.9	6.92/6.72
mixing mechanism				
INHOMO	68.9/86.3	72.9/66.7	11.7/11.0	7.03/6.87

https://doi.org/10.5194/acp-2019-1063
Preprint. Discussion started: 3 December 2019

Atmospheric Chemistry and Physics
Discussions

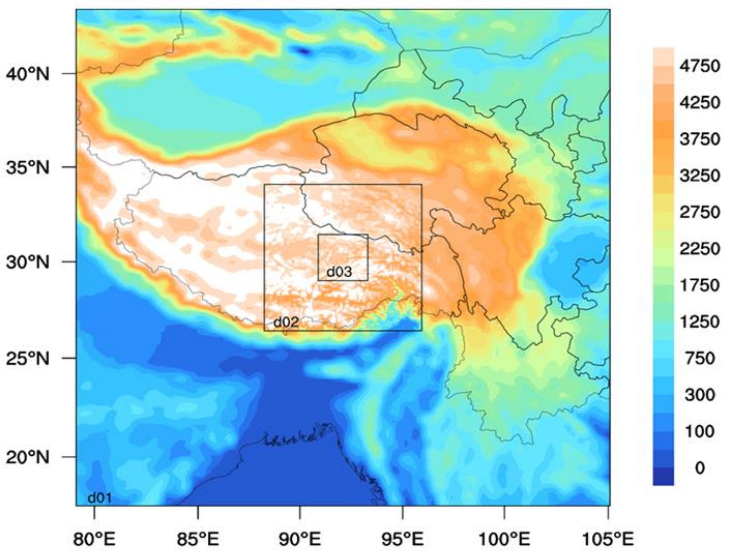

Figure 1. Geographic locations of the three domains used in the numerical simulation.

https://doi.org/10.5194/acp-2019-1063
Preprint. Discussion started: 3 December 2019

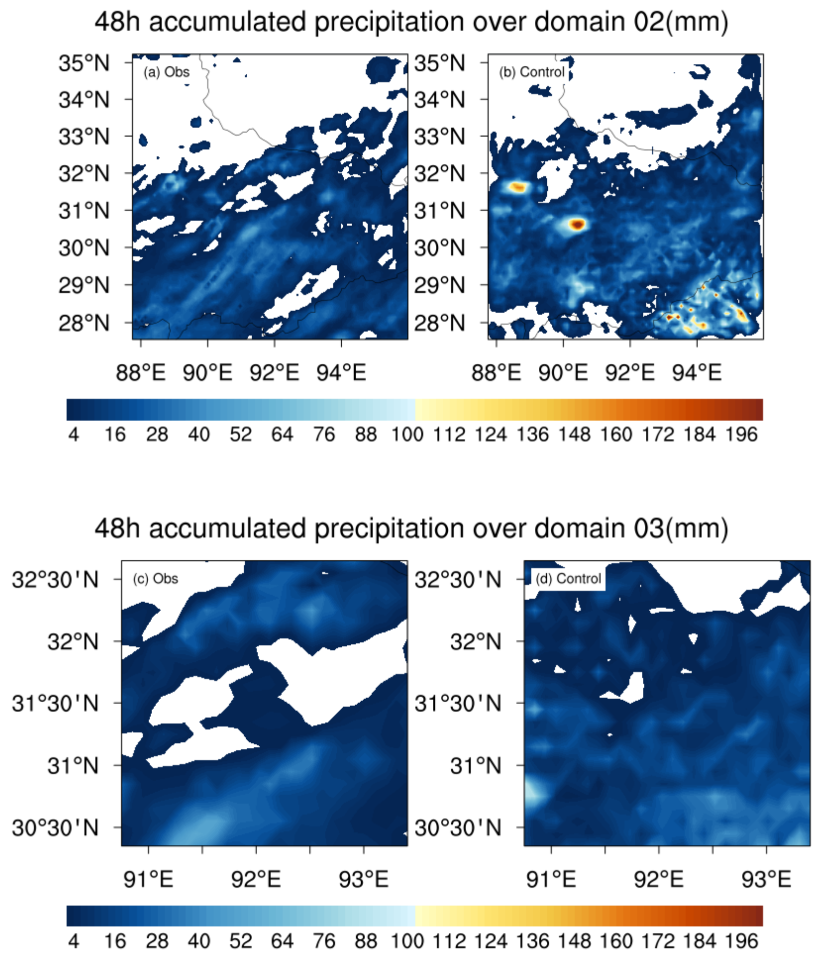

Figure 2. Spatial distributions of 48 h accumulated precipitation (mm) during 0000 UTC 22 July to 0000 UTC 24 July 2014 from the observations and the control run over domain 02 (a, b) and domain 03 (c, d).

https://doi.org/10.5194/acp-2019-1063
Preprint. Discussion started: 3 December 2019

Atmospheric Chemistry and Physics Discussions

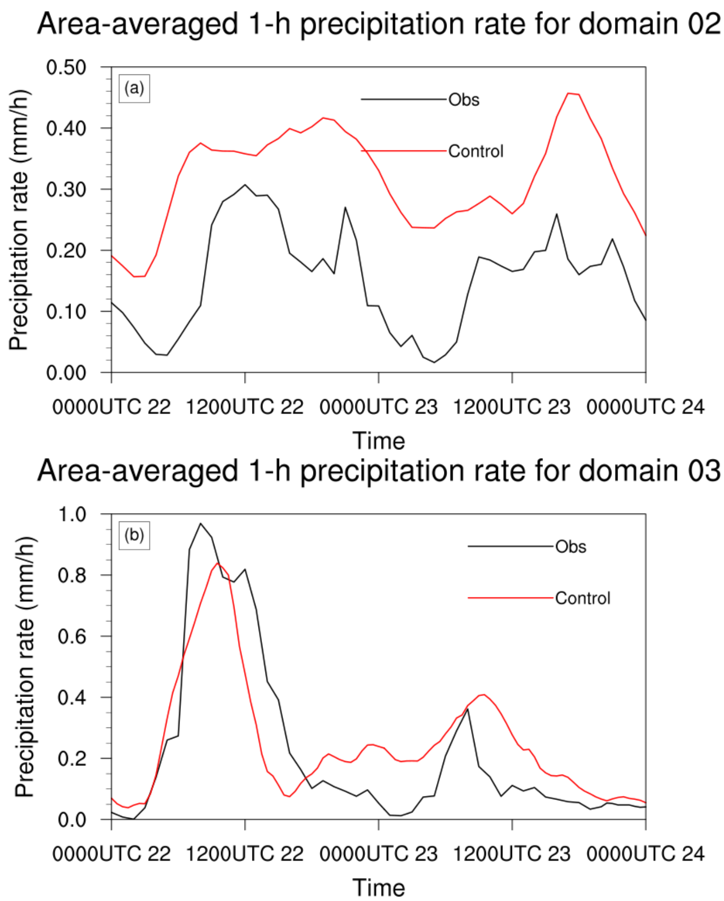

Figure 3. Time series of area-averaged hourly precipitation rate (mm/h) during 0000 UTC 22 July to 0000 UTC 24 July 2014 over (a) domain 02 and (b) domain 03 from the observations and the control run.

https://doi.org/10.5194/acp-2019-1063
Preprint. Discussion started: 3 December 2019

Atmospheric Chemistry and Physics Discussions

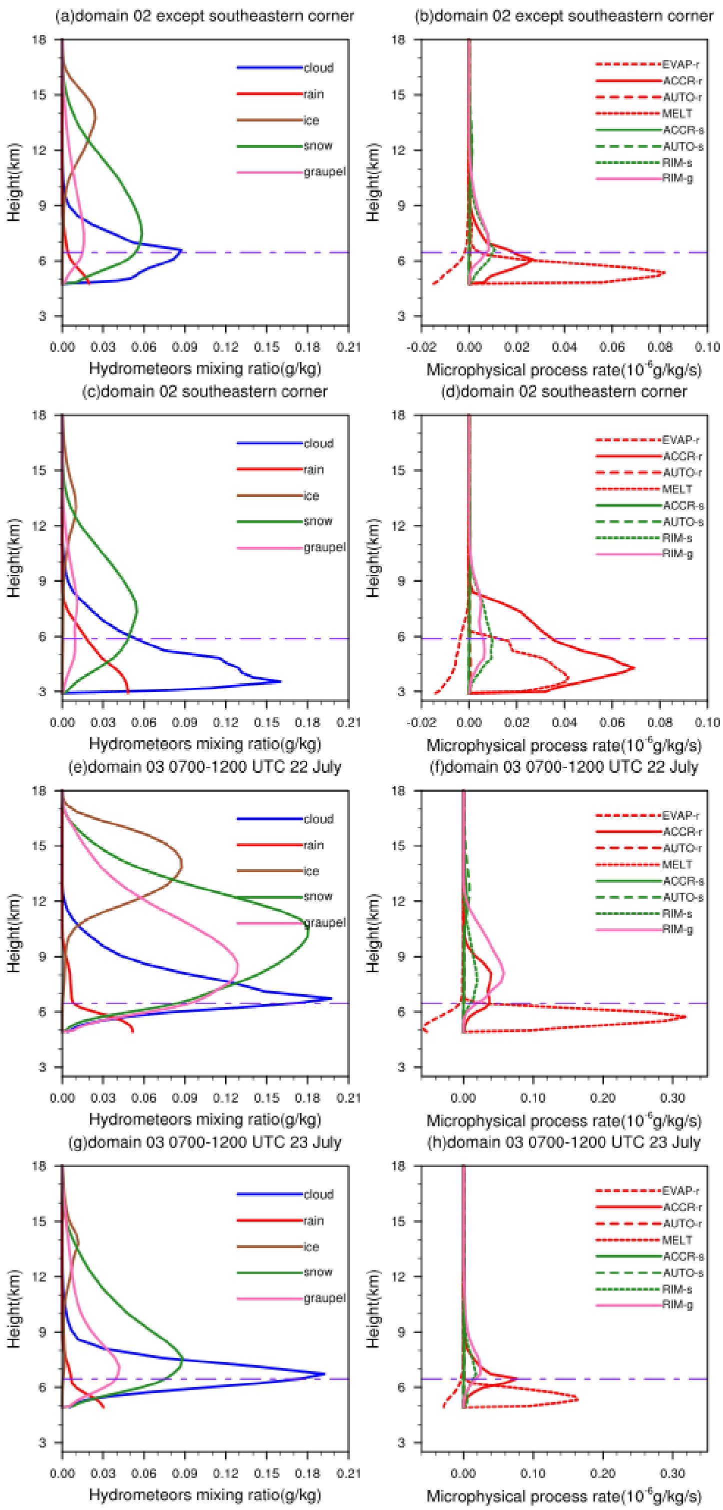

https://doi.org/10.5194/acp-2019-1063
Preprint. Discussion started: 3 December 2019

Atmospheric Chemistry and Physics Discussions
Open Access

Figure 4. Mean vertical profiles of mixing ratios (g/kg) of cloud droplets (q_c), raindrops(q_r), ice particles(q_i), snow particles (q_s), graupel particles(q_g) and their primary microphysical processes in the control run (a, b) averaged from 48 h over domain 02 except southeastern corner, (c, d)averaged from 48 h at southeastern corner over domain 02, averaged during two precipitation peaks (e, f) 0700-1200 UTC 22 July 2014 and (g, h) 0700-1200 UTC 23 July 2014 over domain 03. The purple dot-dash lines denote the mean height of 0 ℃ isotherm. The meanings of the symbols in the legends are shown in Appendix A.

https://doi.org/10.5194/acp-2019-1063
Preprint. Discussion started: 3 December 2019

Atmospheric Chemistry and Physics
Discussions

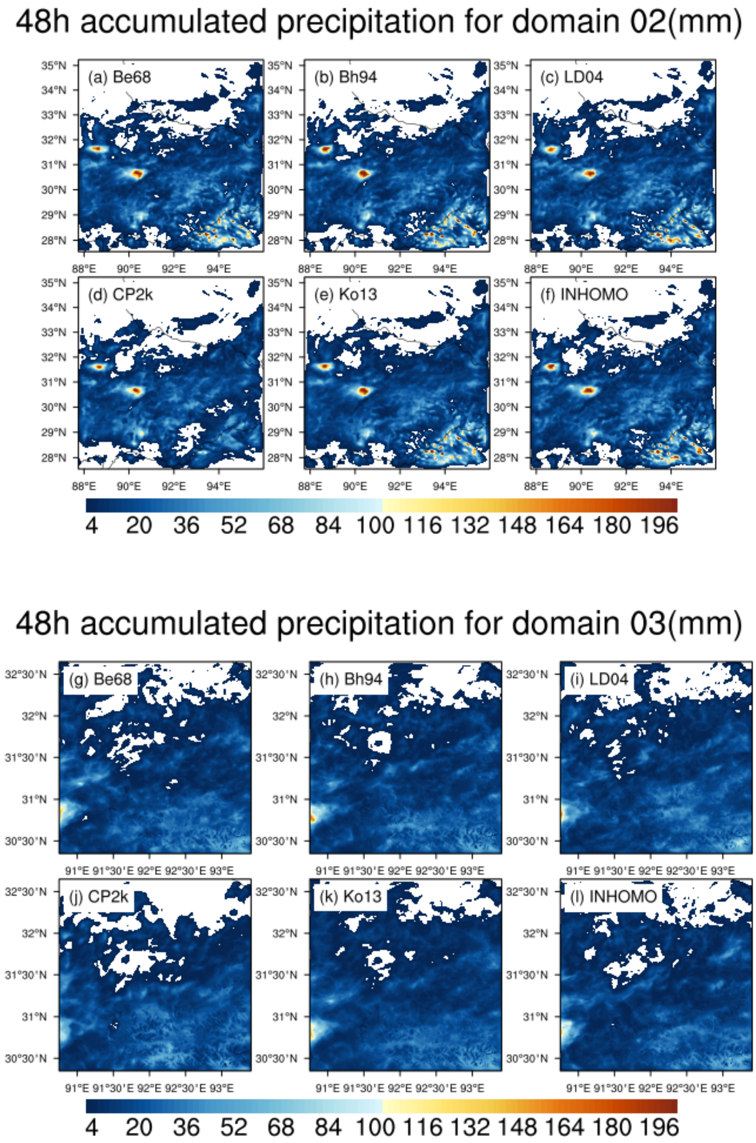

Figure 5. Spatial distributions of 48 h accumulated precipitation (mm) during 0000 UTC 22 July to 0000 UTC 24 July 2014 from observations and all sensitivity simulations over (a-f) domain 02 and (g-l) domain 03.

https://doi.org/10.5194/acp-2019-1063
Preprint. Discussion started: 3 December 2019

Atmospheric Chemistry and Physics Discussions
Open Access
EGU

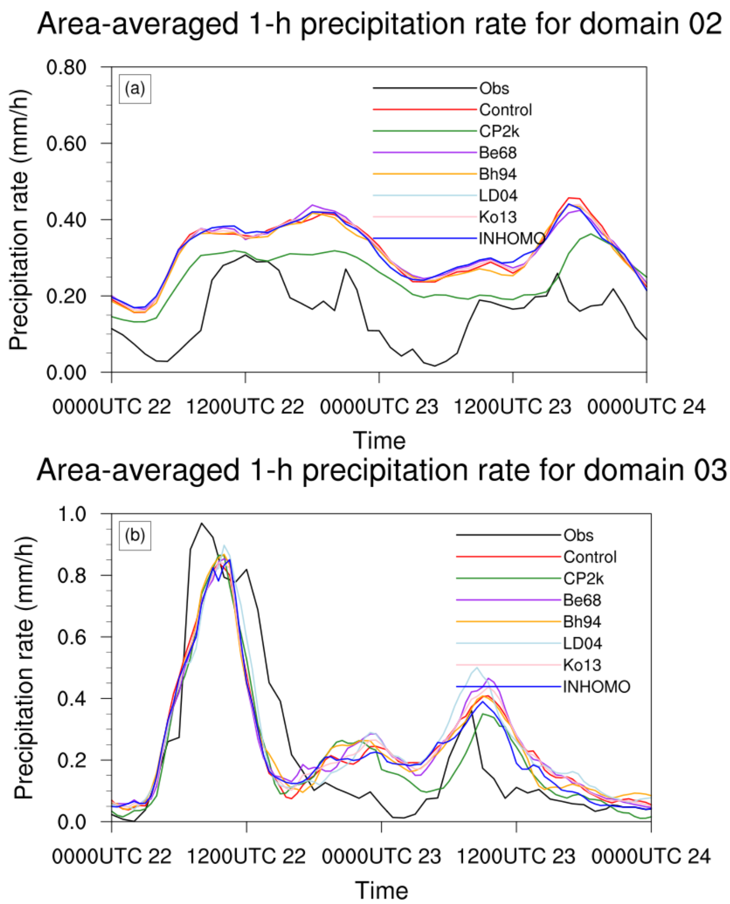

Figure 6. Time series of area-averaged hourly precipitation rate (mm/h) during 0000 UTC 22 July to 0000 UTC 24 July 2014 over (a) domain 02 and (b) domain 03 from the observations and all simulations.

https://doi.org/10.5194/acp-2019-1063
Preprint. Discussion started: 3 December 2019

Atmospheric Chemistry and Physics Discussions

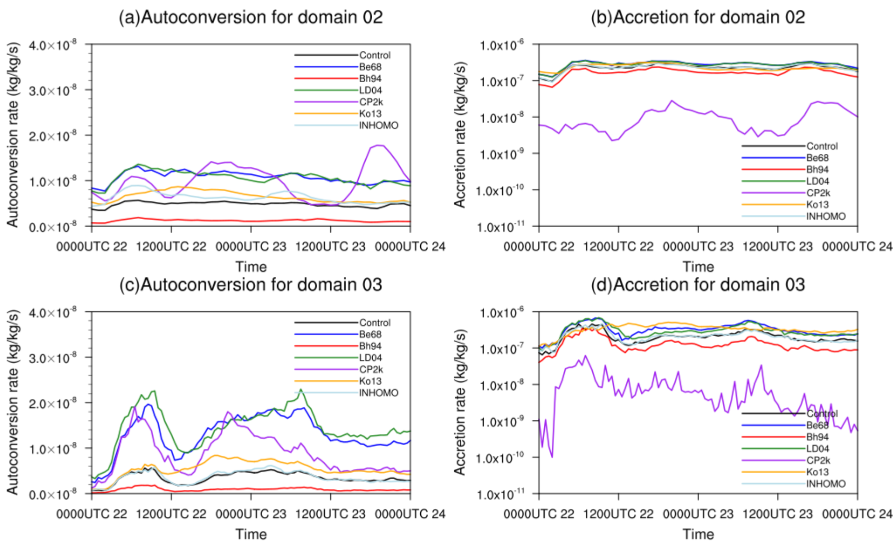

932

933 Figure 7. The time series of area-averaged autoconversion rate and accretion rate over

934 (a, b) domain 02 and (c, d) domain 03 for all simulations, respectively.

935

https://doi.org/10.5194/acp-2019-1063
Preprint. Discussion started: 3 December 2019

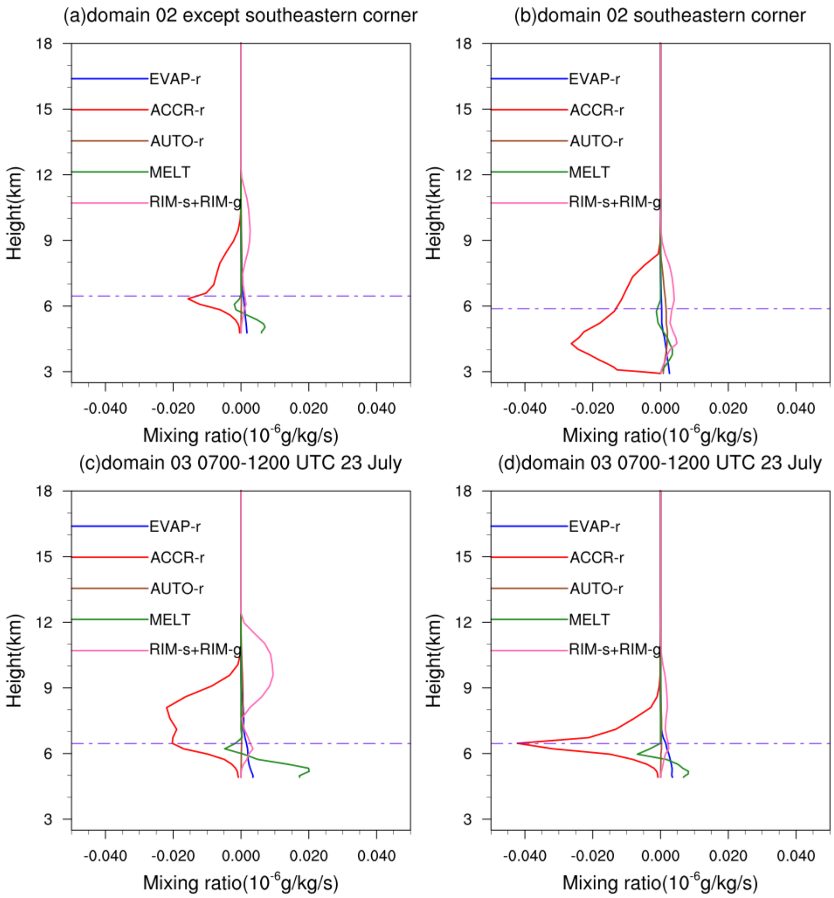

Figure 8. Differences of mean vertical profiles of the dominated microphysical processes conversion rates between the CP2k and the control run (CP2k-Control) from (a) domain 02 except southeastern corner, (b) the southeastern corner of domain 02, and during the two precipitation peak periods (c) 0700-1200 UTC 22 July and (d) 0700-1200 UTC 23 July over domain 03. The purple dot-dash lines denote the mean height of 0 °C isotherm. The meanings of the symbols in the legends are shown in Appendix A.

https://doi.org/10.5194/acp-2019-1063
Preprint. Discussion started: 3 December 2019

Atmospheric Chemistry and Physics Discussions

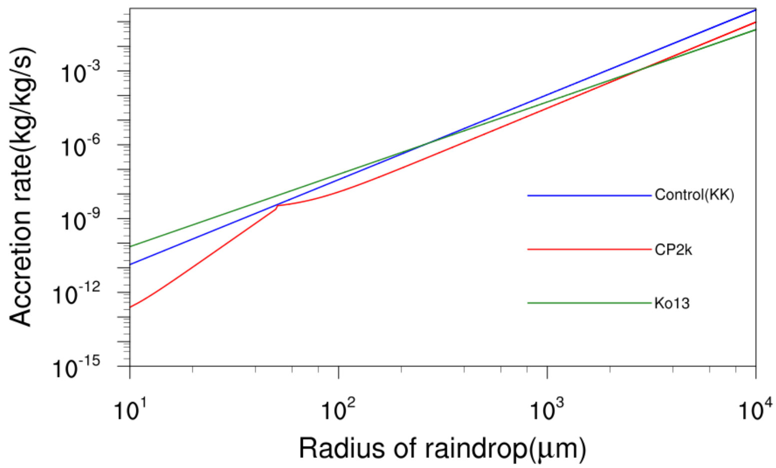

946
947 Figure 9. The accretion rate as a function of raindrop radius with fixed cloud mixing
948 ratio q_c = 1 g/kg, the radius of cloud droplet R_c = 10 μm, number concentration of
949 raindrops N_r = 4000 /m^3 for the three accretion schemes.
950

https://doi.org/10.5194/acp-2019-1063
Preprint. Discussion started: 3 December 2019

Atmospheric Chemistry and Physics Discussions

951
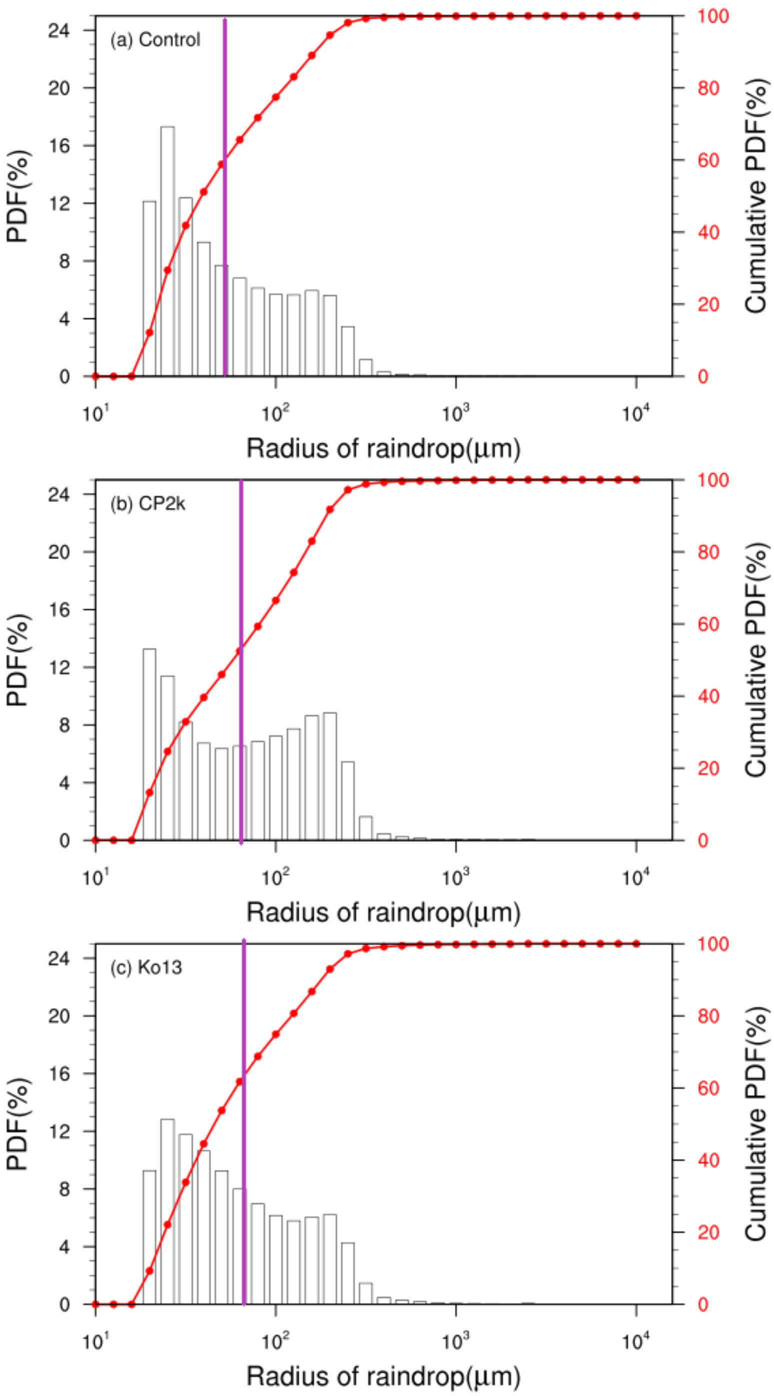

952 Figure 10. Probability distribution function (PDF) and cumulative PDF of raindrop

https://doi.org/10.5194/acp-2019-1063
Preprint. Discussion started: 3 December 2019

Atmospheric Chemistry and Physics Discussions

radius involved in the accretion process for (a) the control run, (b) the CP2k, and (c) the Ko13. The purple line denotes the radius of raindrop equal to 50 μm.

https://doi.org/10.5194/acp-2019-1063
Preprint. Discussion started: 3 December 2019

Atmospheric Chemistry and Physics
Discussions

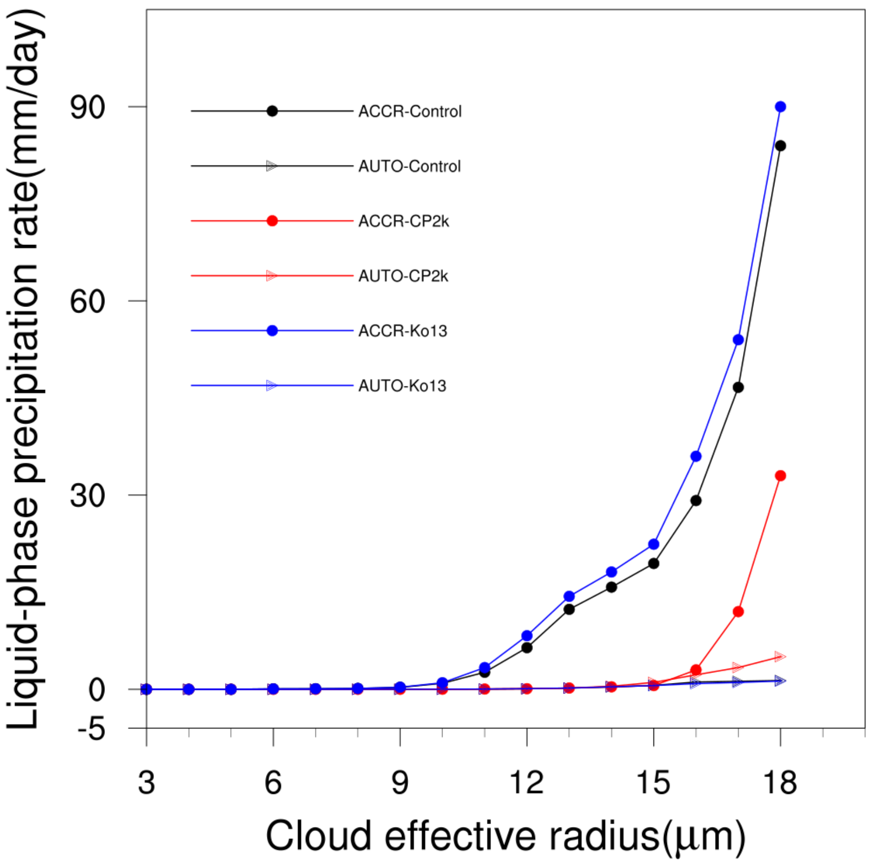

956

957 Figure 11. Dependence of liquid-phase precipitation intensity on cloud effective radius

958 from the three accretion schemes during 0000 UTC 22 July to 0000 UTC 24 July 2014

959 over domain 03.

960